Supporting Information

Synergism between metal single-atom sites and S-vacated two-dimensional nanosheets for efficient hydrogen evolution uncovered by density functional theory and machine learning

Xinyi Li[a], Dongxu Jiao[a], Jingxiang Zhao[*,b], Xiao Zhao[*,a]

a. Key Laboratory of Automobile Materials of MOE, School of Materials Science and Engineering, Jilin University, Changchun 130012, China

b. College of Chemistry and Chemical Engineering, and Key Laboratory of Photonic and Electronic Bandgap Materials, Ministry of Education, Harbin Normal University, Harbin 150025, China.

Email: xzhao417@jlu.edu.cn; zhaojingxiang@hrbnu.edu.cn

Computational Details

CHE model

According to previous studies, the hydrogen adsorption free energy (ΔG_{H^*}) can be widely accepted as a good descriptor to evaluate the HER catalytic activity on a given catalyst, which is defined as follows: $\Delta G_{H^*} = \Delta E_{H^*} + \Delta E_{ZPE} - T\Delta S_H$. In this equation, ΔE_{H^*} is the hydrogen adsorption energy, which is determined by $\Delta E_{H^*} = E_{H^*} - E_{H2/2} - E$cat, where E_{H^*}, $E_{H2/2}$, and Ecat represent the total energies of the adsorbed H^* species, free H_2 molecule, and catalyst, respectively, ΔE_{H^*} and ΔS_H are the differences in zero-point energy and the entropy between the adsorbed state and gas phase, respectively, and T is the temperature. When calculating the total energy of a molecule, we use the harmonic approximation to estimate the zero-point energy (ZPE). The contributions from the catalyst substrate to ΔS_H are very small and negligible, which is thus obtained by $\Delta S_H \approx -1/2 S_{H2}$. Thus, ΔG_{H^*} can be rewritten as $\Delta G_{H^*} = \Delta E_{H^*} + 0.24$ eV according to previous theoretical reports.

The free energy of hydroxyl adsorption is defined as:

$$\Delta G_{OH} = G_{*OH} - G_{*} - G_{OH^-},$$

where G_{*OH}, G_{*} and G_{OH^-} are the free energies of species adsorbed, catalysts, and hydroxyl species. At equilibrium potential of HER: $G_{H_2O} = G_{OH^-} + \frac{1}{2}G_{H_2}$.Thus, $\Delta G_{*OH} = G_{*OH} - G_{*} - G_{H_2O} + \frac{1}{2}G_{H_2}$.

Double-reference method

The solvent environment in the double-reference method was simulated using an implicit solvation model implemented in the VASPsol code, where the relative dielectric constant of water was set to 78.5. To illustrate the energy changes at different potentials, we performed nine independent calculations with system charge from -2 e to 2 e in a step of 0.5 e. The electric potential of the electrochemical interface is changed by adjusting the work function. It could be calculated by:

$$U = (W_f - 4.60) + 0.0592 \times \mathrm{pH}$$

where U is electrode potential referenced to SHE, W_f is the work function and 4.60 is the work function of H_2/H^+ at standard conditions. The work function could be controlled by adjusting the number of charges. When the electrode potential is at a fixed potential on the RHE scale, the electric potential referenced to the SHE scale is also changed by changing the pH values. It was given by:

$$U_{RHE} = U_{SHE} + 0.0592 \times \mathrm{pH}$$

According to Neurock methods, the potential-dependent energy of the system can be calculated by:

$$E_{free}(U) = E_{DFT} + \int_0^q \langle \bar{V}_{tot} \rangle dQ + qW_f$$

where E_{DFT} is the total energy of the unit cell calculated by DFT calculations, $\int_0^q \langle \bar{V}_{tot} \rangle dQ$ and qW_f are considered corrected energies. Specifically, $\int_0^q \langle \bar{V}_{tot} \rangle dQ$ is an integral from 0 to the system charge of the average electrostatic potential in the unit cell

and qW_f is given by the number of electrons (added and removed) multiplied by the work functions.

GBR model:

Machine learning (ML) is based on the gradient-boosted regression (GBR) algorithm. The training set D = {(x_1, y_1), (x_2, y_2), …(x_n, y_n)} is divided into J disjoint parts, where J is the number of leaf nodes in every regression tree. To minimize the loss function L, the decision tree parameter θ_m is defined as:

$$\theta_m = argmin_\theta \sum_{i=1}^{n} L(y_i, f_{m-1}(x_i) + t_m(x_i))$$

Where $t_m(x), f_{m-1}(x)$ is the m_{th} and the $(m-1)_{th}$ regression tree function after iterations. The GRB training process is summarized by four steps: (1) initializing a regression tree function $argmin_\theta \sum_{i=1}^{n} L(y_i,c)$ where c is a constant number. (2) Calculate the negative gradient of the loss function as the estimated residual value r_{mi} = - $[\partial L(y_i, f(x_i)/\partial f(x_i)]_{f(x)=f_{m-1}(x)}$. (3) Use the new data set(x_i, r_{mi}) to obtain the updated regression tree function $f_m(x)$. (4) Repeat steps (2) and (3) to reach the final regression model, which is determined by:

$$f_M(x) = \sum_{m-1}^{M} t(x;\theta m)$$

The prediction accuracy of GBR is described by the coefficient of determination (R^2) and root-mean-square error (RMSE), defined as:

$$R^2 = 1 - \frac{\frac{1}{n}\sum_{i=1}^{n}(y_i - \hat{y}_i)^2}{\frac{1}{n}\sum_{i=1}^{n}(y_i - \mu_i)^2}$$

$$RMSE = \sqrt{\frac{1}{n}\sum_{i=1}^{n}(y_i - \hat{y}_i)^2}$$

In which y_i and $\hat{y}_i$ are the sample label value and the predicted value based on the GBR model, respectively. Usually, a higher R^2 and a lower RMSE mean a more precise GBR model. The coefficient of determination (R^2) and root-mean-square error (RMSE) to evaluate the model accuracy, in which R^2 and RMSE are expected to be close to 1 and 0 for the ideal model. Based on the optimal parameters, the GBR method was used to evaluate the performance of each model. More discussions on the GBR method can be seen in the Supporting Information.

Dissolution Potential.

To evaluate the stability of Pd_1/S_v-$MnPS_3$ monolayer in realistic reaction conditions, such as strong acidic media and working potential, we computed the dissolution potentials (U_{dis}, in V) of Pd in Pd-$MnPS_3$(Sv) monolayer at pH=0, which was defined as: $U_{diss} = U_{Pd}^{0} + \left[E_{Pd,bulk} - \left(E_{Pd_1/S_v-MnPS_3} - E_{S_v-MnPS_3}\right)\right]/2$, where E_{Pd_1/S_v-MnPS_3}, $E_{S_v-MnPS_3}$, $E_{Pd,bulk}$ represent the total energies of Pd_1/S_v-$MnPS_3$ monolayer, S_v-$MnPS_3$ monolayer, and the Pd atom bulk form, U_{Pd}^{0} is the standard dissolution potential of Pd in the bulk form, and 2 is the coefficient for the aqueous dissolution reaction: $Pd + 2H^+ \leftrightarrow Pd^{2+} + H_2$.

Pourbaix diagrams of oxidation potential.

To explore the electrochemical stability of Pd_1/S_v-$MnPS_3$ in an aqueous solvent, the following formulas calculate its possible oxidation states at different pH values respectively Pourbaix diagrams of oxidation potential.

$Pd_1/S_v\text{-}MnPS_3 + H_2O \rightarrow Pd_1\text{-}OH/S_v\text{-}MnPS_3 + H^+ + e^-$

$Pd_1\text{-}OH/S_v\text{-}MnPS_3 \rightarrow Pd_1\text{-}O/S_v\text{-}MnPS_3 + H^+ + e^-$

The Gibbs free energy change (ΔG) of these reactions in a solvent environment can be computed as:

$$\Delta G_1 = G_{Pd_1-OH/S_v-MnPS_3} + \frac{1}{2} G_{H_2} - G_{Pd_1/S_v-MnPS_3} - G_{H_2O} - 0.059pH - eU$$

$$\Delta G_2 = G_{Pd_1-O/S_v-MnPS_3} + \frac{1}{2} G_{H_2} - G_{Pd_1-OH/S_v-MnPS_3} - 0.059pH - eU$$

Where Pd_1-OH/S_v-$MnPS_3$, and Pd_1-O/S_v-$MnPS_3$ denote the substances adsorbed OH^*, and O^* on Pd_1/S_v-$MnPS_3$ catalyst.

Note 1: Due to Tc is radioactive and may cause radiation exposure in an experimental study, and Cd and Ta are inert to HER, these metals are not considered as the potential metal-SAs.

Note 2: The calculated distance between confined metal-SAs and the Mn/Pd atoms is based on their Cartesian coordinates after structural relaxation.

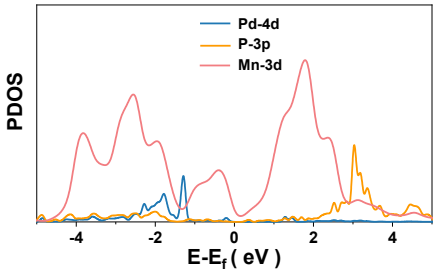

Fig. S1 The computed partial density of states (PDOSs) of the Pd_1/S_v-$MnPS_3$ model.

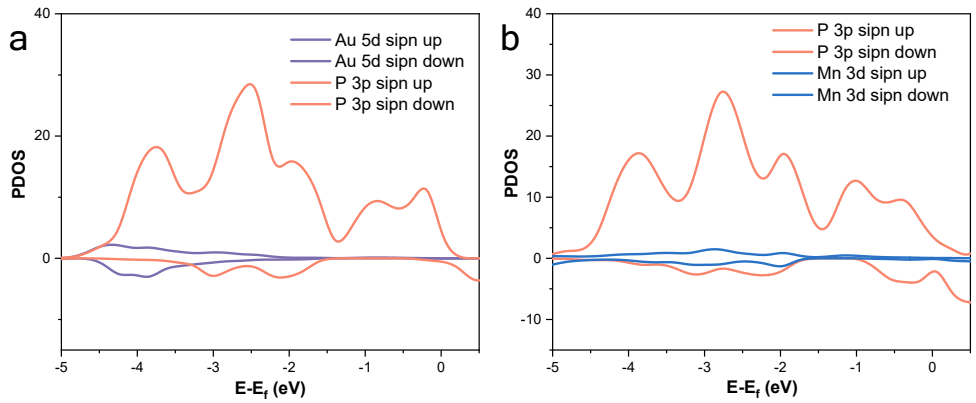

Fig. S2 The computed partial density of states (PDOSs) of the (a) Au_1/S_v-$MnPS_3$ and (b) Mn_1/S_v-$MnPS_3$ model.

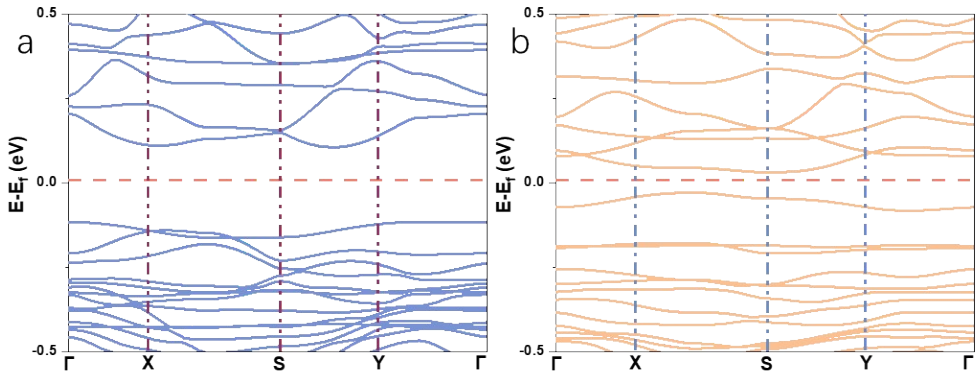

Fig. S3 The computed band structures of the (a) Au_1/S_v-$MnPS_3$ and (b) Mn_1/S_v-$MnPS_3$ model. (The Fermi energy levels are indicated by the red dashed lines.)

Note 3 The Au_1/S_v-$MnPS_3$ and Mn_1/S_v-$MnPS_3$ possess semiconducting properties due to their energy band structures do not cross the Fermi energy level with the band gap of 0.22 and 0.06 eV, respectively.

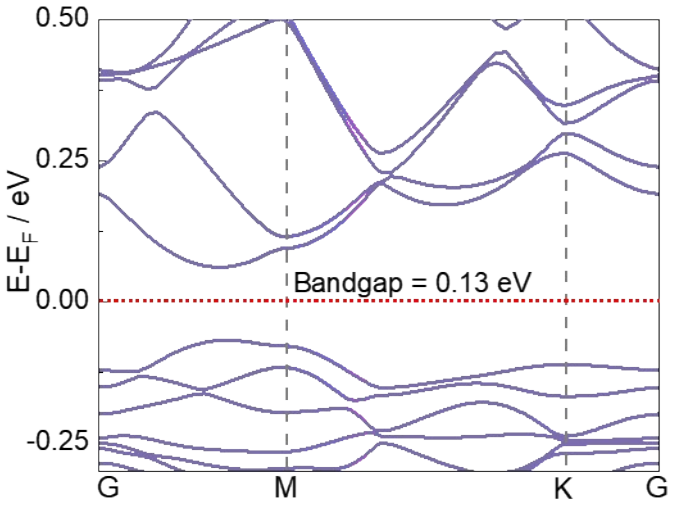

Fig. S4 The computed band structures of the S_v-$MnPS_3$ model. (The Fermi energy levels are indicated by the red dashed lines.)

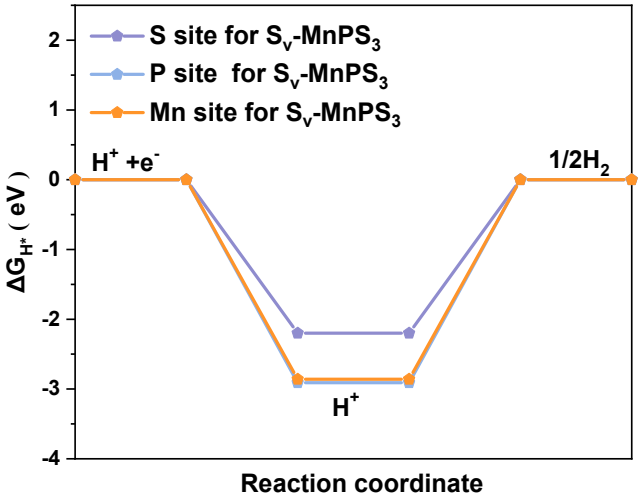

Fig. S5 The Gibbs free energies of H adsorption on S, Mn, and P sites for the S_v-$MnPS_3$ model.

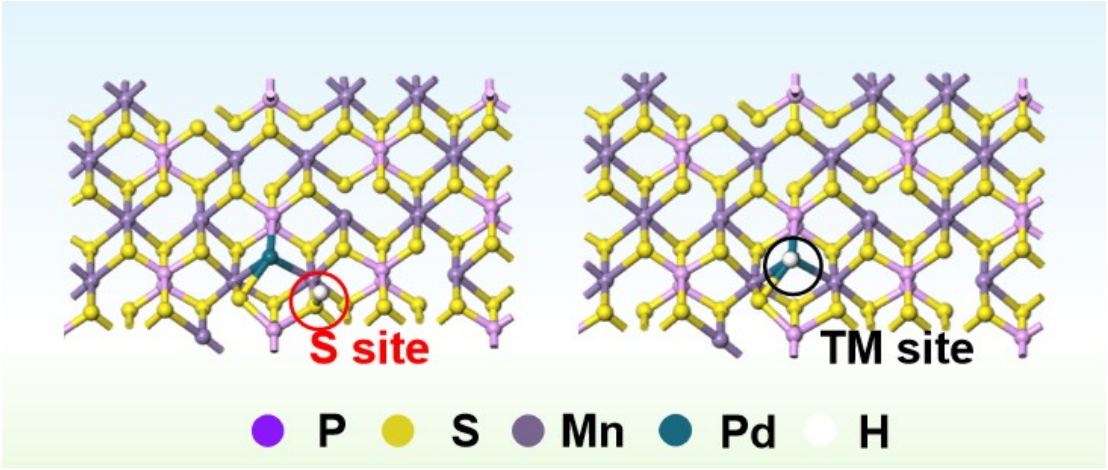

Fig. S6 Configuration diagram considering two possible H adsorption sites, i.e., metal atom sites and S sites adjacent to the metal.

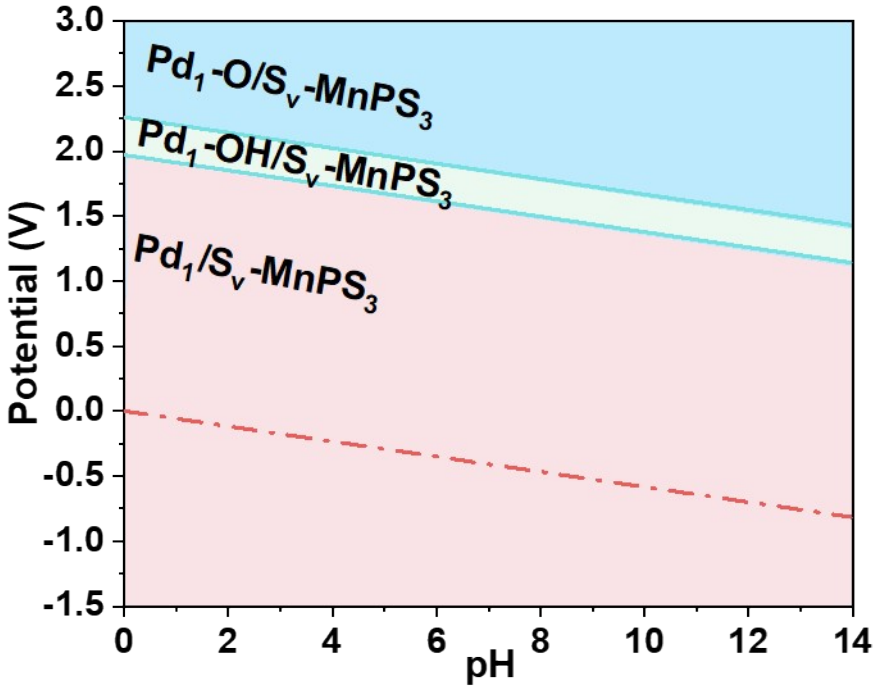

Fig. S7 The computed surface Pourbaix diagram of Pd_1/S_v-$MnPS_3$ catalyst.

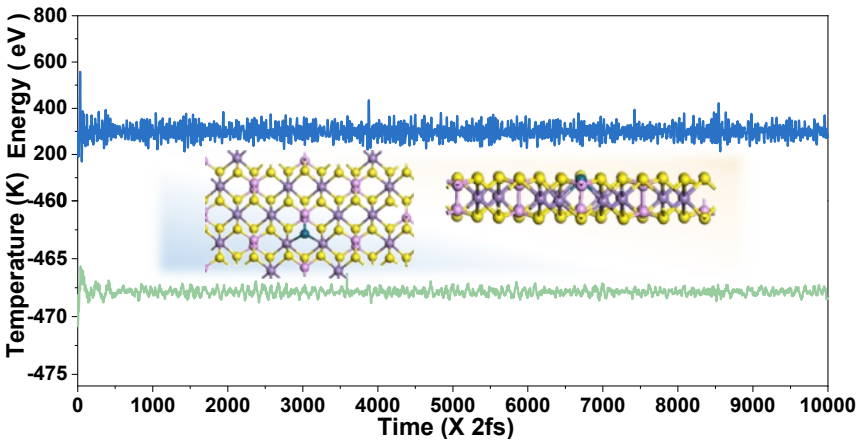

Fig. S8 The variations of temperature and energy versus the time for AIMD simulations of Pd_1/S_v-$MnPS_3$. Schematic diagrams of the atomic configurations after dynamics simulation (top and side views) are also given.

Table S1. The bond lengths between the confined metal-SAs and the Mn/Pd atoms.

Catalysts	$d_{m\text{-}Mn}$/Å	$d_{m\text{-}P}$/Å
Mn_1/S_v-$MnPS_3$	2.37	2.46
Fe_1/S_v-$MnPS_3$	2.62	2.04
Co_1/S_v-$MnPS_3$	2.38	2.20
Ni_1/S_v-$MnPS_3$	2.50	2.18
Cu_1/S_v-$MnPS_3$	2.56	2.24
Ru_1/S_v-$MnPS_3$	2.35	2.25
Rh_1/S_v-$MnPS_3$	2.58	2.26
Pd_1/S_v-$MnPS_3$	2.64	2.25
Pt_1/S_v-$MnPS_3$	2.60	2.19
Cr_1/S_v-$MnPS_3$	2.42	2.44
Ir_1/S_v-$MnPS_3$	2.47	2.18
Mo_1/S_v-$MnPS_3$	2.38	2.55
Os_1/S_v-$MnPS_3$	2.41	2.21
Re_1/S_v-$MnPS_3$	2.18	2.43
W_1/S_v-$MnPS_3$	2.36	2.51
Hf_1/S_v-$MnPS_3$	2.42	2.67
Nb_1/S_v-$MnPS_3$	2.54	2.62
Sc_1/S_v-$MnPS_3$	2.51	2.78
Ti_1/S_v-$MnPS_3$	2.24	2.62
V_1/S_v-$MnPS_3$	2.41	2.51
Zn_1/S_v-$MnPS_3$	2.61	2.45
Zr_1/S_v-$MnPS_3$	2.43	2.70
Ag_1/S_v-$MnPS_3$	2.60	2.41
Au_1/S_v-$MnPS_3$	2.67	2.34

Table S2. The computed charge transfer (Q), the d-band center (ε_d), the bond length of active atoms and adsorbed H species (d), and the magnetic moment of metal atoms (μ_B) in intermediates.

Catalysts	Q / e$^-$	ε_d / eV	μ_B	d/Å
^{as}Mn/S_v-$MnPS_3$	1.11	-0.96	4.26	1.57
^{as}Fe/S_v-$MnPS_3$	0.11	-0.93	2.19	1.55
^{as}Co/S_v-$MnPS_3$	0.09	-0.86	0.75	1.56
^{as}Ni/S_v-$MnPS_3$	0.11	-0.88	0.04	1.54
^{as}Cu/S_v-$MnPS_3$	0.10	-2.46	0.06	1.52
^{as}Ru/S_v-$MnPS_3$	0.40	-1.20	0.17	1.53
^{as}Rh/S_v-$MnPS_3$	0.04	-1.31	0.14	1.57
^{as}Pd/S_v-$MnPS_3$	0.16	-2.06	0.20	1.54
^{as}Pt/S_v-$MnPS_3$	0.43	-2.50	0.33	1.82
^{as}Au/S_v-$MnPS_3$	0.28	-4.58	0.09	1.61
^{as}Cr/S_v-$MnPS_3$	0.71	-2.45	2.83	1.60
^{as}Hf/S_v-$MnPS_3$	1.27	-7.1	0.02	1.86
^{as}Ir/S_v-$MnPS_3$	0.27	-7.19	0.33	1.59
^{as}Mo/S_v-$MnPS_3$	0.73	-2.85	0.86	1.73
^{as}Nb/S_v-$MnPS_3$	1.10	-4.01	0.25	1.80
^{as}W/S_v-$MnPS_3$	0.84	-8.20	0.92	1.74
^{as}Os/S_v-$MnPS_3$	0.05	-8.50	0.07	1.63
^{as}Re/S_v-$MnPS_3$	0.39	-7.54	0.32	1.76
^{as}Sc/S_v-$MnPS_3$	1.32	-4.02	0.11	1.81
^{as}Ti/S_v-$MnPS_3$	1.02	-7.5	0.01	1.73
^{as}V/S_v-$MnPS_3$	0.92	-5.33	0.21	1.70
^{as}Zn/S_v-$MnPS_3$	0.29	-7.41	0.04	1.55
^{as}Zr/S_v-$MnPS_3$	1.24	-7.23	0.28	1.36

$^{as}Ag/S_v$-$MnPS_3$	0.54	-3.45	0.07	1.64
$Mn/^{as}S_v$-$MnPS_3$	0.95	-1.20	4.28	1.36
$Fe/^{as}S_v$-$MnPS_3$	0.09	-0.60	2.28	1.32
$Co/^{as}S_v$-$MnPS_3$	0.09	-0.92	0.99	1.34
$Ni/^{as}S_v$-$MnPS_3$	0.11	-2.06	0.59	1.40
$Cu/^{as}S_v$-$MnPS_3$	0.12	-0.52	0.35	1.38
$Ru/^{as}S_v$-$MnPS_3$	0.32	-0.30	0.15	1.35
$Rh/^{as}S_v$-$MnPS_3$	0.06	-2.99	0.27	1.36
$Pd/^{as}S_v$-$MnPS_3$	0.15	-1.24	0.40	1.33
$Pt/^{as}S_v$-$MnPS_3$	0.41	-1.61	0.02	1.34
$Au/^{as}S_v$-$MnPS_3$	0.25	-4.22	0.01	1.35
$Cr/^{as}S_v$-$MnPS_3$	0.75	-2.54	1.93	1.36
$Hf/^{as}S_v$-$MnPS_3$	1.23	-5.80	0.02	1.37
$Ir/^{as}S_v$-$MnPS_3$	0.23	-6.20	0.12	1.36
$Mo/^{as}S_v$-$MnPS_3$	0.56	-1.85	0.15	1.36
$Nb/^{as}S_v$-$MnPS_3$	0.95	-3.58	0.34	1.36
$W/^{as}S_v$-$MnPS_3$	0.82	-7.50	1.01	1.35
$Os/^{as}S_v$-$MnPS_3$	0.06	-6.50	0.01	1.37
$Re/^{as}S_v$-$MnPS_3$	0.51	-5.85	0.30	1.35
$Sc/^{as}S_v$-$MnPS_3$	1.43	-4.32	0.14	1.36
$Ti/^{as}S_v$-$MnPS_3$	1.20	-5.62	0.11	1.37
$V/^{as}S_v$-$MnPS_3$	1.02	-5.45	2.26	1.36
$Zn/^{as}S_v$-$MnPS_3$	0.62	-7.02	0.02	1.37
$Zr/^{as}S_v$-$MnPS_3$	1.33	-6.85	0.24	1.36
$Ag/^{as}S_v$-$MnPS_3$	0.34	-3.52	0.01	1.35